MEASUREMENT SCIENCE REVIEW, **17**, (2017), No. 4, 197-207

DE GRUYTER OPEN

MEASUREMENT SCIENCE REVIEW

Journal homepage: http://www.degruyter.com/view/j/msr

ISSN 1335-8871

Measuring Software Test Verification for Complex Workpieces based on Virtual Gear Measuring Instrument

Peili Yin, Jianhua Wang, Chunxia Lu

Xi'an Technological University, School of Mechatronic Engineering, No.2 Middle of Xuefu Road, 710021, Xi'an, Shaanxi, PR China, wangjianhuaxatu@126.com

Validity and correctness test verification of the measuring software has been a thorny issue hindering the development of Gear Measuring Instrument (GMI). The main reason is that the software itself is difficult to separate from the rest of the measurement system for independent evaluation. This paper presents a Virtual Gear Measuring Instrument (VGMI) to independently validate the measuring software. The triangular patch model with accurately controlled precision was taken as the virtual workpiece and a universal collision detection model was established. The whole process simulation of workpiece measurement is implemented by VGMI replacing GMI and the measuring software is tested in the proposed virtual environment. Taking involute profile measurement procedure as an example, the validity of the software is evaluated based on the simulation results; meanwhile, experiments using the same measuring software are carried out on the involute master in a GMI. The experiment results indicate a consistency of tooth profile deviation and calibration results, thus verifying the accuracy of gear measuring system which includes the measurement procedures. It is shown that the VGMI presented can be applied in the validation of measuring software, providing a new ideal platform for testing of complex workpiece-measuring software without calibrated artifacts.

Keywords: Software testing, complex workpiece, Virtual Gear Measuring Instrument (VGMI), collision detection, triangular patch.

1. INTRODUCTION

Since the 1980s when the GMI was first introduced, its application has expanded sprawling to gears represented by complex cutting tools, worm gears and worms. Compared with the traditional instrument, the GMI has the advantages of complete software function, high measuring precision and high efficiency. As the mechanical structure and the control system of the GMI are no longer immature, its function expansion and precision improvement lies mainly in the development of measurement software [1]. However, the validity and correctness verification of the developed software has been a thorny issue hindering the development of gear measurement instruments [2]-[7].

Frazer proposed that the software is very difficult to evaluate independently of the rest of the measurement system [8]. The testing of software is usually included in the complete measurement system testing process. At present, the overall measurement accuracy of any measuring system in the GMI depends largely on the testing repeatability and reproducibility of physical standards in a strictly controlled testing environment, such as the involute master [9], the helix master [9], the Double Ball Artifact (DBA) [10], and the wedge artifact [11]. The measurement results would be compared against either standard calibration certificates or other different apparatuses. However, different apparatus makers may adopt different measurement strategies, mathematical models and computing methods in their respective workpiece measurement software development, inevitably resulting in some major differences between experimental results from testing GMIs of different apparatus makers, even on the same workpiece [12]. Unlike most of the concept of physical quantities, software quality cannot be traced to any measurement standards [5]. Therefore, it is necessary to establish a method to detect and evaluate the measuring software quality independently.

The independent test designed for coordinate measuring software is centered on the testing of the evaluation algorithm. The test method for Gaussian fitting calculation of general element has been specified in ISO 10360-6 [13]. PTB and NIST have respectively designed the standard test data and reference software for the least-squares fitting evaluation algorithm used for the coordinate measuring system [14], [15]. By preparing a set of standard test data, PTB researched into the involute cylindrical gear evaluation software and established the evaluation on the assessment algorithm after obtaining the measurement data [12]. The software certification in discussion is applicable to the robustness test of the parameter evaluation but does not work for the algorithm with non-calibrated artifacts. Yet, another independent test remains to be done for firmware deviations from CNC controller occurring in driving machine, measurement data gathering and implementation

DOI: 10.1515/msr-2017-0023

[8]. Fumi Takeoka [16] proposed a Virtual Gear Checker (VGC) to simulate gear measurement. Its working principle is to solve the contact problem of the probe and the measured surface described by theoretical equations. It enables the analysis of the effects of the error factors on the gear checker and the estimation of the uncertainty.

This paper proposes a VGMI (Virtual Gear Measuring Instrument) and a digital measuring model to solve the aforementioned problems. Theoretical verifiability of VGMI and errors design characteristics of the digital measuring model could be used for gear measurement software validation. The discretization of virtual workpiece with controllable errors is presented and a collision detection algorithm independent from the workpiece surface is established to construct the VGMI. The measuring software of the real GMI can be used to propel directly the VGMI to simulate the measurement of the digital standard workpiece. By taking measuring procedures of the involute tooth profile deviation as an example, this paper tests and verifies the measurement software by both simulation and experiment.

2. VIRTUAL GEAR MEASURING INSTRUMENT SYSTEM

2.1. VGMI system concept

VGMI system represents the mapping of the real GMI's mechanical structure, working performance and measuring process in the computer environment. It replaces the real GMI and makes the integrated simulation analysis of the measuring process possible. Establishing a VGMI system enables in-depth studies of features and functions of the real GMI.

As shown in Fig.1., a GMI is composed of the upper computer, the numerical control system and the mechanical system. To best reflect the structure and metrological characteristics of the real GMI, the VGMI system is divided into three parts: upper computer, VGMI, and virtual workpieces. The VGMI simulates the mechanical system and the numerical control system of the real GMI. The virtual workpiece uses the digital model to replace the actually-processed workpiece to be measured. The measuring software of the upper computer is used to propel either the real GMI or the VGMI. The architecture of the VGMI system is shown in Fig.2.

The workpiece models can be loaded through a simulated interface of VGMI. On the VGMI, the geometric error, motion error, probe error and others can be input and set up via relevant human machine interface. The measurement motion and data collecting, processing and evaluating are controlled by the software of the upper computer through the virtual interface of the VGMI, and eventually, a range of measurement reports can be produced by adjusting parameters for different measuring purposes.

The VGMI will be used to conduct a simulated measuring of workpiece at a precision P_{ref}, the result of which, denoted by Result P, will be compared with the design indices P_{ref}. The evaluation of measuring software will be done based on the test metric δ. The flow chart of testing the measuring software by VGMI is shown in Fig.3.

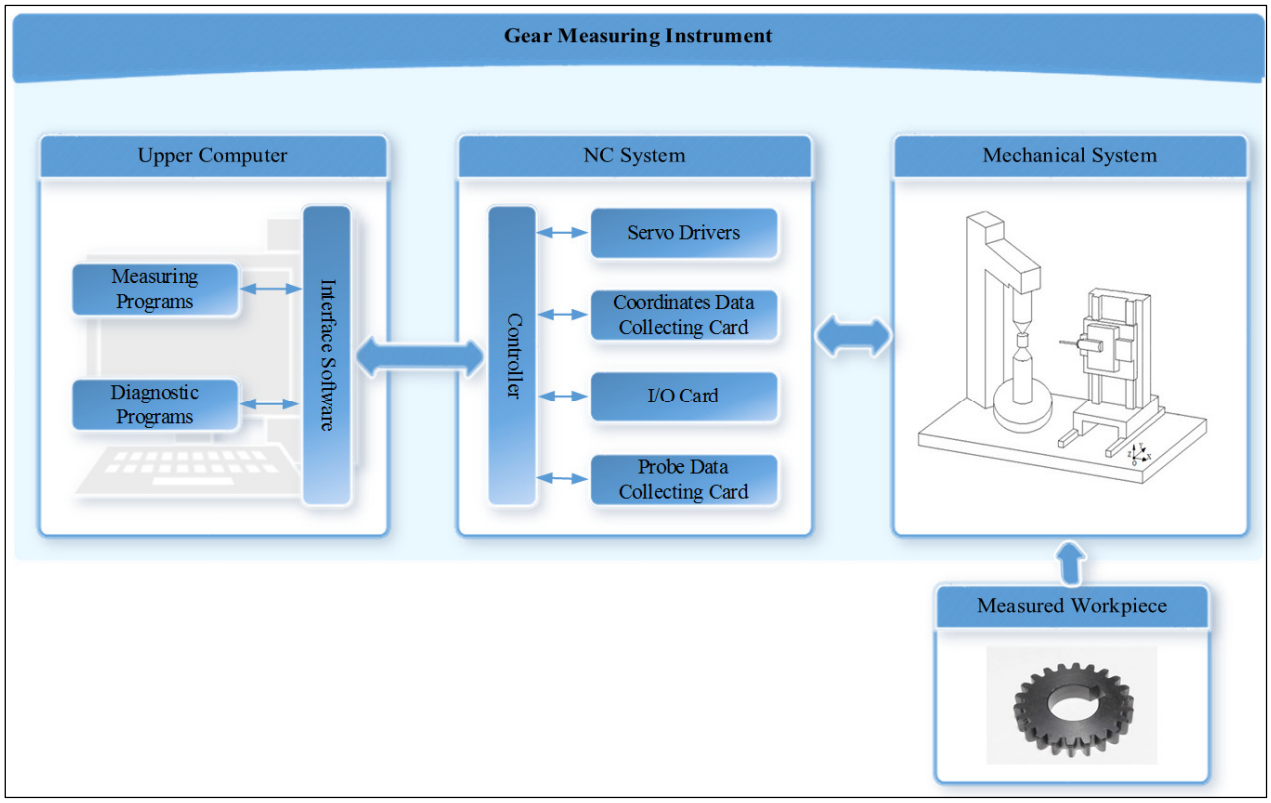

Fig.1. Real GMI architecture.

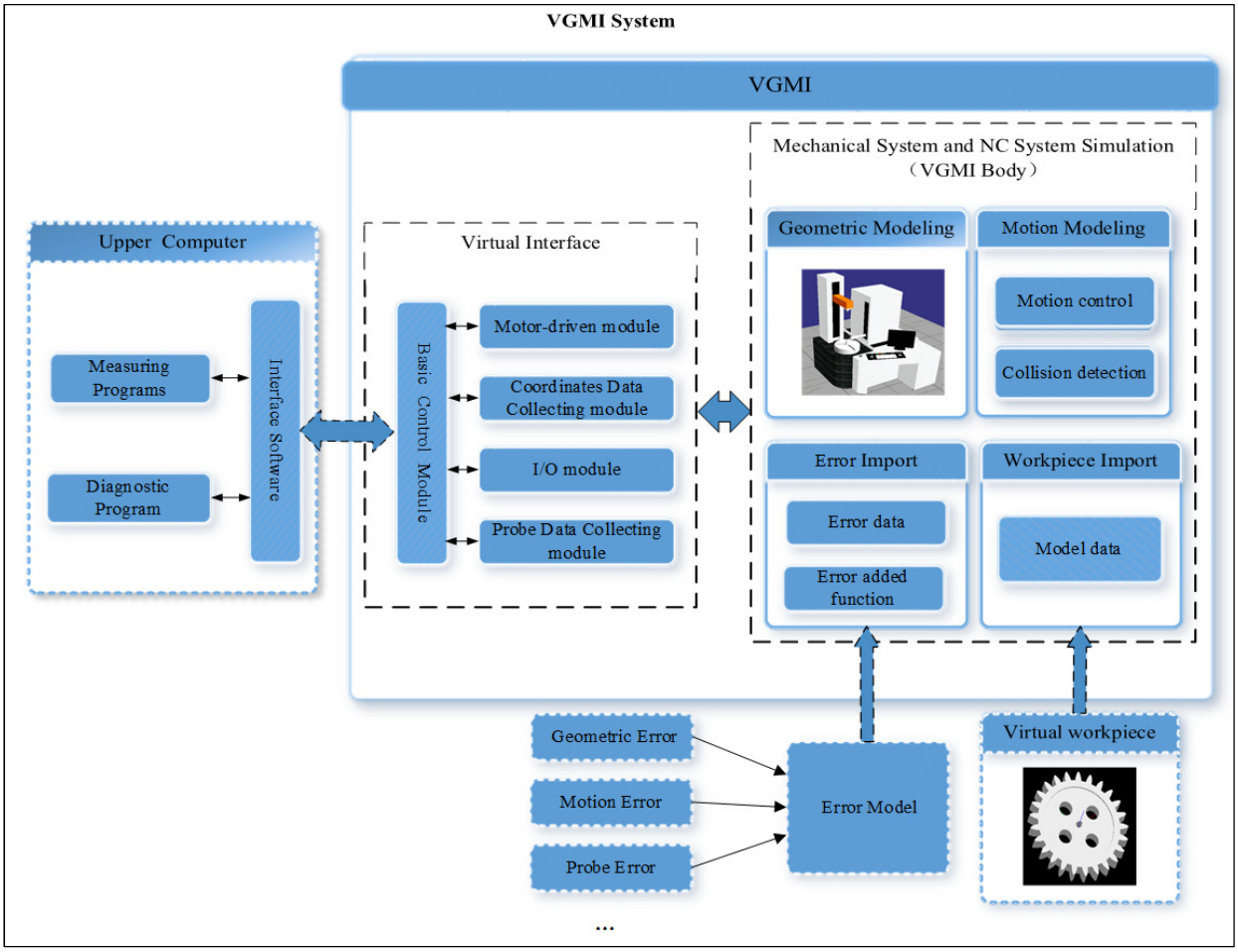

Fig.2. Architecture of the proposed VGMI system.

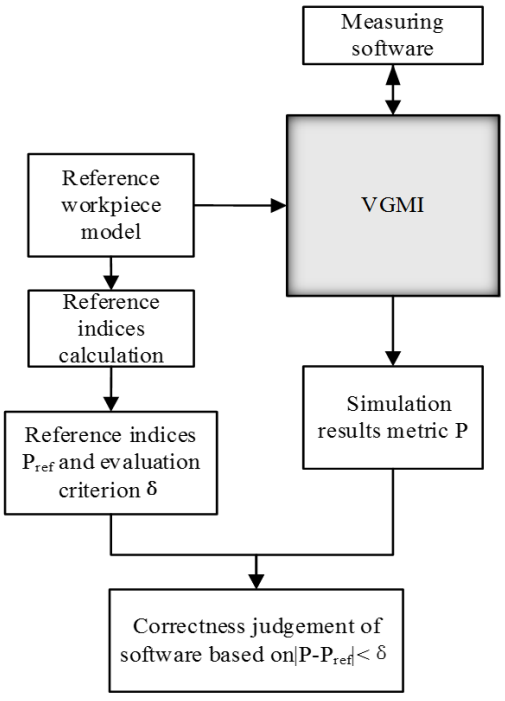

Fig.3. Flowchart of testing the measuring software by VGMI.

2.2. Technical details

2.2.1. Construction of virtual workpiece

Virtual workpiece is the object of virtual measurement, and its theoretical design precision is the comparison standard with VGMI simulation results. In order to meet the testing requirements of VGMI software, a constructor of triangular-facet mesh orderly arranged in high precision is presented here. The virtual workpiece built by the presented method has three characteristics: (1) the precision of models could accurately be determined; (2) triangular patch sets could represent any complex workpiece models, so different workpiece models will be unified into a set of triangles; (3) the model represented by the triangular patch is free from the theoretical model adopted in the measuring procedures so that the errors occurring in the measuring software can be detected.

The mathematical workpiece model, studied with analytical method or numerical method, is used to calculate the surface discrete nexus, and the construction should be done based on the data structure of STL models. When constructing the triangular-facet mesh, the quantity of tri-patches used should be decided accordingly by the physical models' surface complexity and required measurement accuracy.

For a complicated surface model, it is difficult to find out the mathematical relationship between triangle numbers and quantization error, though any complicated surface model can be interpreted by the subdivision method. When the first selected subdivided surface grid vertex density fails to meet the given accuracy, it is necessary to further subdivide the triangle mesh. As shown in Fig.4., midpoints at each edge of the triangle on the surface are chosen as a new vertex. Connect the new vertex with the other two vertices on the same triangle edge, and link three new vertices. Finally, by removing the original three triangle edges, four subdivided triangle meshes are formed.

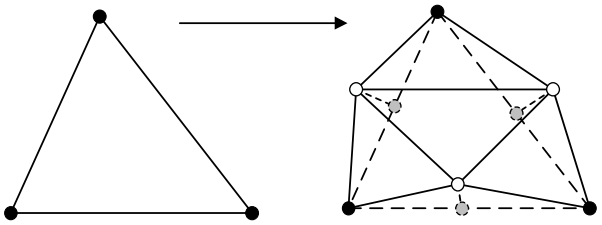

Fig.4. 1-4 subdivision rules of triangular element.

The subdividing accuracy can be measured by controlling the distance between mesh triangle patch and its corresponding patch. For the C^2 continuous parametric surface S(u,v)， (u,v)∈Ω， $l_i(u,v)$ is the interpolated *i*-th triangular patch, and Ω_i is the triangular domain of the three vertices P_i^0、P_i^1、and P_i^2 of the *i*-th triangular patch. Then $l_i(P_i^j)=S(P_i^j)$， *j*=0,1,2. The error bound of the *i*-th triangular surface approximation to the parametric surface e_i is as:

$$e_i=\sup_{(u,v)\in\Omega_i}\left\|S(u,v)-l_i(u,v)\right\| \tag{1}$$

e_i can be quickly estimated as [17]:

$$e_i=\sup_{(u,v)\in\Omega_i}\left\|S(u,v)-l_i(u,v)\right\|\le\frac{1}{8}L_i^2(M_1+M_2+M_3-\min(M_1,M_2,M_3)) \tag{2}$$

where

$$M_1=\sup_{(u,v)\in\Omega_i}\left\|\frac{\partial^2S(u,v)}{\partial u^2}\right\|,$$

$$M_2=\sup_{(u,v)\in\Omega_i}\left\|\frac{\partial^2S(u,v)}{\partial u\partial v}\right\|,$$

$$M_3=\sup_{(u,v)\in\Omega_i}\left\|\frac{\partial^2S(u,v)}{\partial v^2}\right\|.$$

L_i is the longest edge of triangle Ω_i .

When determining the accuracy of the workpiece model discretization, it requires a refined calculation of e_i. The geometrical meaning of e_i is the distance between the furthest point - P_{imax} on the surface S(u,v) to the triangle $P_i^0P_i^1P_i^2$ within the Ω_i domain. P can be calculated from

$$\begin{cases} n(u,v)=\dfrac{r_u\times r_v}{\left\|r_u\times r_v\right\|}=\dfrac{\overrightarrow{P_i^0P_i^1}\times\overrightarrow{P_i^0P_i^2}}{\left\|\overrightarrow{P_i^0P_i^1}\times\overrightarrow{P_i^0P_i^2}\right\|} \\ S(u_{i\max},v_{i\max})=0 \end{cases}, \tag{3}$$

where $r_u=\dfrac{\partial S(u,v)}{\partial u}, r_v=\dfrac{\partial S(u,v)}{\partial v}$.

According to the distance formula of point to triangle, e_i can be accurately obtained as follows:

$$e_i=\frac{\left\|\overrightarrow{P_{i\max}P_i^0}\bullet n(u_{i\max},v_{i\max})\right\|}{\left\|n(u_{i\max},v_{i\max})\right\|} \tag{4}$$

The triangle patch of the parametric surface approximates δ_c, the maximum error value of its corresponding surface, which is:

$$\delta_c=\left\|\begin{matrix}e_0\\e_1\\\vdots\\e_i\\\vdots\\e_n\end{matrix}\right\|_\infty. \tag{5}$$

2.2.2. Collision detection model

The module of VGMI collision detection is the core of the motion modeling. It mainly simulates the collision detection between the probe and the workpiece in the real GMI, examines whether there is any collision between the probe and the workpiece in the virtual space and assesses the collision if there really is one. Judging from the Sec. 2.2.1., we may infer that the detection algorithm for a collision between the virtual probe and the complex virtual workpiece applies also to a collision between the probe and the triangular patch sets. In other words, it is also the algorithm for positional relations between the probe and the simple triangular patch that could lead to vectors of touch measurement. The collision detection model has the following advantages: (1) The collision detection model is uniform and simple. For different workpiece models, only considering the collision detection between the virtual probe and the simple triangular face set, we do not need to establish different collision detection models for different analytical surfaces. (2) The workpiece model used in collision detection model differs from the mathematical model of workpiece in the measurement procedures, which can separate measurement software error caused by the problem of mathematical model of workpiece.

The complex spatial collision detection algorithm could be simplified in two steps: first, figure out the projection point of the virtual probe center to the nearest triangular patch; second, convert the distance between the projection point and the probe center into touch measurement vector in line with the direction of touch measurement. How the collision between the virtual probe and the virtual workpiece is like can be evaluated by comparing the distance between the probe center and the nearest point of the workpiece surface and the probe radius.

By projecting the center point P of the ball onto the plane of ΔABC, it can be divided into seven characteristic domains: one surface (F), three edges (E1, E2, E3) and three vertices (V1, V2, V3), as shown in Fig.5. In order to find out the nearest point Q in ΔABC from P, the first step is to estimate which domain of the triangle P belongs to, and then project P orthogonally into this domain. As is shown in Fig.6, the domain of vertex A can be regarded as the intersection VR(A) of negative half space between plane $(X-A)\cdot(B-A)=0$ and plane $(X-A)\cdot(C-A)=0$.

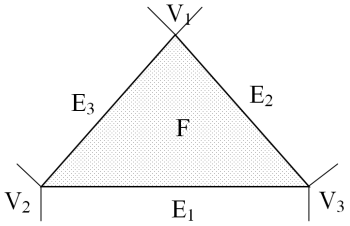

Fig.5. Characteristic domains of triangle.

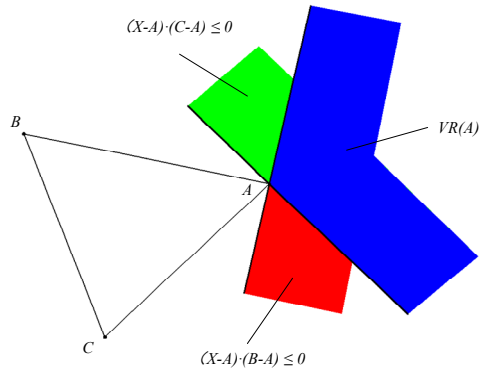

Fig.6. Vertex domain of point A.

The conditions for determining when P locates at A's vertex domain are:

$$\begin{cases}(X-\mathrm{A})\cdot(\mathrm{B}-\mathrm{A})\le 0\\(X-\mathrm{A})\cdot(C-\mathrm{A})\le 0\end{cases}. \tag{6}$$

The conditions for determining when point P locates at the vertex domains of point B and C can be obtained similarly.

The conditions for determining that P locates at AB's edge domain are:

$$\begin{cases}(\overrightarrow{PA}\times\overrightarrow{PB})\cdot\vec{n}\le 0\\(X-A)\cdot(B-A)\ge 0\\(X-B)\cdot(A-B)\ge 0\end{cases}. \tag{7}$$

Among them, $\vec{n}$ is the unit normal vector of the measured triangle vector.

The conditions for determining when point P locates at the edge domains of BC and AC can be obtained similarly.

If point P is found neither in the vertex domain nor the edge domain, P is surely located at the surface domain of ΔABC.

After determining P's location in the triangle domains, an orthogonal projection of it onto the domain will reveal the nearest point Q. The Q's coordinates can be calculated according to Q's barycentric coordinates（a,b,c）.

$$Q=aA+bB+cC \tag{8}$$
$$a=\frac{(\overrightarrow{PB}\times\overrightarrow{PC})\cdot\vec{n}}{\left\|\overrightarrow{AB}\times\overrightarrow{AC}\right\|},\ b=\frac{(\overrightarrow{PC}\times\overrightarrow{PA})\cdot\vec{n}}{\left\|\overrightarrow{AB}\times\overrightarrow{AC}\right\|},$$
$$c=\frac{(\overrightarrow{PA}\times\overrightarrow{PB})\cdot\vec{n}}{\left\|\overrightarrow{AB}\times\overrightarrow{AC}\right\|}$$

The touch measurement vector $\overrightarrow{Pr}$ is calculated by taking the vector of the probe center P to the projection point Q as the real probe direction.

$$\overrightarrow{Pr}=R\cdot\frac{\overrightarrow{QP}}{\left\|\overrightarrow{QP}\right\|}-\overrightarrow{QP}. \tag{9}$$

where R represents the sphere radius. When QP<R, it means that the probe and the workpiece surface had contact-wise collision and the touch measurement vector can be calculated through the formulae (9).

3. VGMI SIMULATION TEST

3.1. Parameter settings of virtual workpiece and VGMI

For the involute tooth surface STL model, the involute accuracy of any of its axis cross sections is the same, and the precision expressed by the chord height difference is the maximum error of the curve fitting involute line. The method of equal arc length is used to divide the discrete points on the involute. According to the method in Sec. 2.2.1., with the span segments P_{1ref} and the profile accuracy P_{2ref} as the reference index and using simulated tooth profile accuracy δ as the evaluation standard, a tooth surface model can be constructed, with an accuracy of 14.52 um, 4.83 um, and 0.99 um, respectively, and it is correspondingly cut into 12, 25, 72 segments along the span. The design parameters of the involute master are shown in Table 1. The resolution parameters of the acquisition system of VGMI system are shown in Table 2.

δ represents the absolute value of the maximum permissible error in VGMI's error measurement of tooth profile. The errors of VGMI system mainly come from the indication error caused by the resolution of the acquisition system. A total differential of tooth profile deviation formula results in the df calculation formula of tooth profile:

$$df = d\Delta T - r_b d\Delta\theta + d\Delta S\,, \tag{10}$$

where $d\Delta T$ is the sampling error of the T axis and its value is ±0.2 um; $d\Delta\theta$ is the angle sampling error of the rotary shaft, and its value is ±0.0000061 rad; $d\Delta S$ is probe sampling error and its value is ±0.015 um. Substituting each value into the above equation will yield a df value of ±0.5 um. Therefore, the maximum permissible error (MPE) of VGMI simulated tooth profile deviation measurement system is ±0.50 um, thus the standard measuring value δ of the tooth profile deviation is ±0.50 um.

Table 1. Design parameters of the involute master.

Parameters	Value
Involute initial rolling length	0 mm
Involute end rolling length	30 mm
Base circle radius	46.985 mm
Tooth width	100 mm
Helix angle	0°
Number of tooth width division	Model 1 : 3 segments Model 2 : 3 segments Model 3 : 3 segments
Number of rolling length division P_{1ref}	Model 1 : 12 segments Model 2 : 25 segments Model 3 : 72 segments
Calibrated value of tooth profile deviation P_{2ref}	Model 1 : 14.52 um Model 2 : 4.83 um Model 3 : 0.99 um
Probe diameter	Spherical probe ϕ3 mm

Table 2. Resolution parameters of VGMI acquisition system.

Parameters	Value
Resolution of T axis	0. 2 um
Resolution of R axis	0. 2 um
Resolution of Z axis	0. 2 um
Resolution of rotary axis	0.0000061 rad
Resolution of probe	0.015 um

The VGMI visualization model is shown in Fig.7. Fig.7. consists of the VGMI's geometry model, workpiece model, visualization scene, operator panel, real-time motion coordinates and collision detection information, etc. The upper right corner of it is the partially enlarged detail of the collision detection between virtual probe and virtual workpiece. The bottom of it is the display of VGMI real-time motion coordinates and touch-sensitive vector.

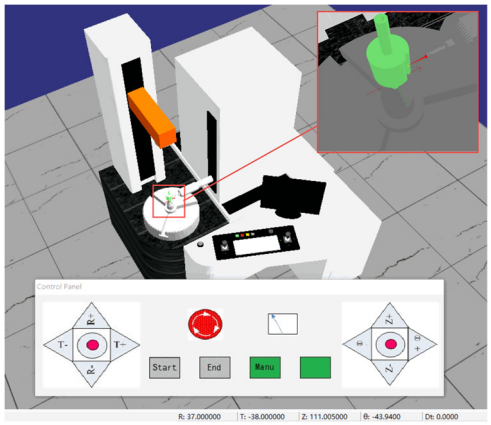

Fig.7. VGMI and operational user interface.

3.2. VGMI simulation process

The operation of the VGMI system is similar to that of the actual gear measurement instrument. First step is to conduct a simulated measurement of virtual workpiece with a design accuracy of P_{ref}, yielding a simulated value P. Then calculate P's relative difference value compared with P_{ref}. Finally, a comparison between the relative difference value and measuring standard δ would prove the validity of measuring software. The working flowchart of VGMI is shown in Fig.8. Fig.8. explains the concrete workflow of VGMI in Fig.3.

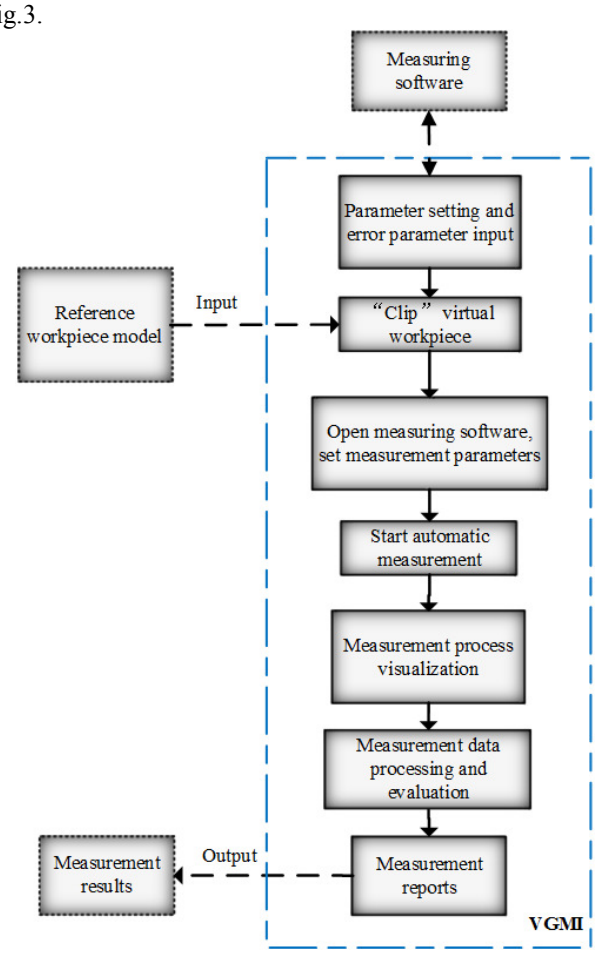

Fig.8. VGMI workflow diagram.

3.3. Simulation results

In the ideal environment of VGMI, the simulation of different precision involute masters is carried out. The involute master of each value needs to be measured five times, based on which the mean value is calculated. The tooth deviation measuring results are shown in Table 3. Fig.9. shows the simulated measuring results of the right tooth profile deviation of the involute master with different accuracy. In order to observe the burr amplitude of the curve, the curve segment was amplified locally, as shown in Fig.9.

It can be seen from Table 3.. that the maximum difference value between P, the simulated tooth profile value acquired from measurement of the tooth profile with three different accuracies, and P_{2ref} , the accuracy index, is 0.48 um, less than the standard value 0.50 um. It can be seen from Fig.10. that the tooth profile error curves are divided into different accuracies exhibiting a fluctuating trend with smaller and smaller fluctuation range as the rolling length increases. With increasing division precision, the fluctuation range of the error curves gets smaller and the error curves get closer to the zero line. The extreme points of the error curves all appear in the first trough. There appear many burrs in the error curve with high noise, which is characterized by higher harmonics, an amplitude of about 0.5 um, as is shown in partial enlarged drawing of Fig.9.This is mainly caused by the resolution of the acquisition system set by VGMI.

The distance between the error curve and the zero-error contour in Fig.9. is the difference between the involute surface and the theoretical involute surface. As the triangular facets are divided into smaller and smaller parts, the fluctuation range of the error data was decreasing with higher accuracy, which objectively shows the surface characteristics of the gear involute, as shown in Fig.10. Measurement results of tooth profile error coincide with the trend that the approximation error varies for triangular patches instead of involute surface, and each trough value represents the maximum chord length of each segment of the rolling length. With the improvement of the accuracy of the tooth surface STL model, the deviation curve wave is getting smaller and smaller, tending to a straight line.

Table 3. Tooth profile deviation measuring results of involute masters with different accuracy.

	Fitting segments P_{1ref}	**Reference accuracy P_{2ref} (um)**	**Simulated Deviation P (um)**	**Difference $P-P_{2ref}$ (um)**	**Evaluation metric δ (um)**	**Estimate**
Model 1	12	14.52	14.90	0.48	0.50	Conformity
Model 2	25	4.83	5.19	0.36		Conformity
Model 3	72	0.99	1.36	0.37		Conformity

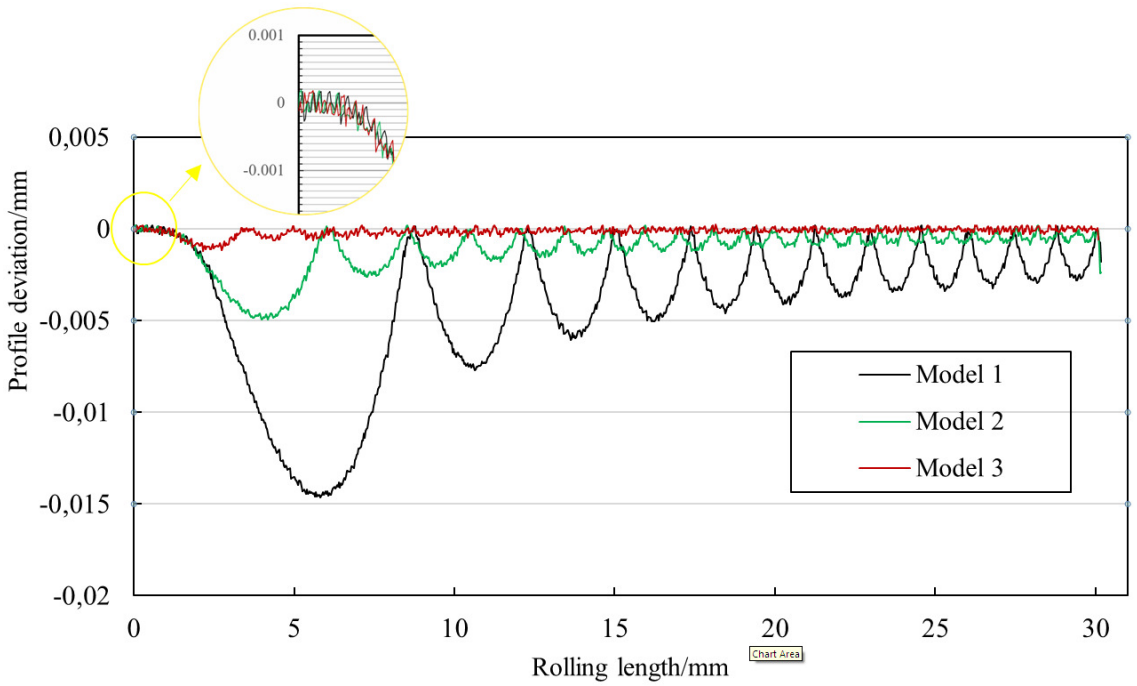

Fig.9. Tooth profile error curves of different accuracy models.

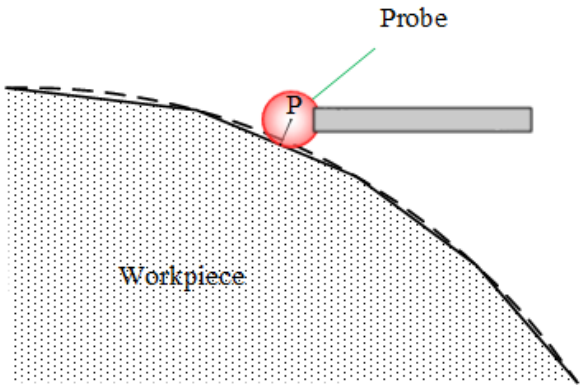

Fig.10. Tooth profile deviation measurement of tooth surface STL model simulation diagram.

Compared with the two indices of the three simulated involute masters' tooth models -rolling length subdivision segments P_{1ref}={12, 25,72} and tooth profile accuracy P_{2ref}={14.52, 4.83, 0.99}, the simulated tooth profile total deviation measuring result- P={14.52, 4.83, 0.99} show relative difference value within the standard 0.5 um. The simulated involute master's span segment numbers are reflected in the simulated tooth profile deviation curve. For instance, there are 12 troughs in the tooth profile deviation curve with 12 segments, which meets the theoretical accuracy index P_{1ref}. This is because when the virtual probe moves along the theoretical measurement path, it inevitably causes indication error, while each point in the error curve can be calculated by surface discretization error formula. Table 3. and Fig.9. fully explain the quantization error occurring when designing the triangular-facet mesh that can be accurately detected by measuring software, which is also an indication that the measuring software can accurately measure the involute tooth surface models with different accuracy. This also proves the validity of involute tooth profile measuring software on a basis of the theoretical simulation.

The above simulated measuring results independently prove the validity of the tooth profile deviation measuring software in theory. The following experiment is conducted to prove the validity of the whole measuring system of the GMI, which includes the tooth profile measuring software.

4. EXPERIMENT

The purpose of this experiment is to prove the validity of the whole measuring system of the GMI, which includes the tooth profile measuring software. The experiment facility used here is the GMC D30 (product of Xi'an Qinchuan Siyuan Measuring Instrument Co., LTD), which shares the same parameters and the same simulated tooth profile deviation measuring software as VGMI. The chosen workpieces are tooth involute master of gear with the same parameters in simulated measuring. The experiment should be carried out in a thermostatic laboratory, measuring the left tooth profile deviation of the involute masters fixed in different positions. The calibration parameters of involute master and major measuring parameters are shown in Fig.4. The fixation of the master in the GMI is shown in Fig.11.

The experimental procedures are as follows:

1. The gear involute masters should be placed in a thermostatic laboratory (20.1 ℃) for more than 4 hours, making sure the templates' temperature is the same as the temperature in the GMI.
2. Place the master ball onto the surface of the rotary table. Set the workpiece coordinate system through the zero correction procedures from two different angles.
3. Fix the involute master between the tips of the up and down of the table in the GMI. Use the tips and clamping drive to firmly clamp and fixate the template.
4. Measure the left tooth profile deviation of the involute master for five times, and save the measuring results. One of the measurement results is shown in Fig.12. Unfix the template, re-fix in a different angle and repeat the process.

Repeat the fix, unfix and re-fix of the gear involute master thirteen times, and average the five measuring results of each fixation. Table 5. shows the tooth profile total deviation, shape deviation and slope deviation of the thirteen fixations. Based on the data from Table 5., the curves drawn of the form deviation and slope deviation of the thirteen fixation experiments are shown in Fig.13. and Fig.14., respectively.

Table 4. Calibration parameters and actual measurement parameters.

Parameters	**Value**
Calibration temperature	20.1 ℃
Material of master	Steel
Base Diameter r_b	46.985 mm
Modulus m	4.000000 mm
Number of teeth Z	25
Pressure angle α	20°
Tooth width	100 mm
Calibration value of profile slope deviation	0.0 um
Calibration value of total profile deviation	0.5 um
Calibration value of profile form deviation	0.5 um
Calibration uncertainty U	1.2 um（k=3）
Evaluation position	Involute rolling length（11-25）mm
Probe diameter	Spherical probe ϕ3 mm
Actual measured temperature	20.1±0.2 ℃

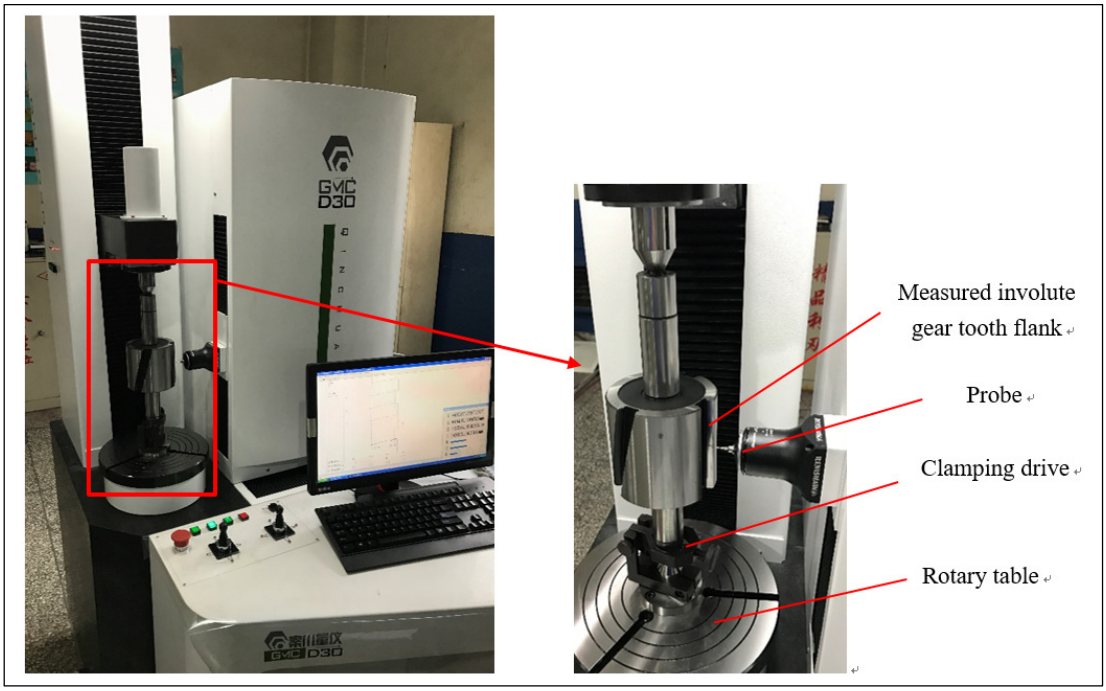

Fig.11. Experimental equipment and installation of involute master.

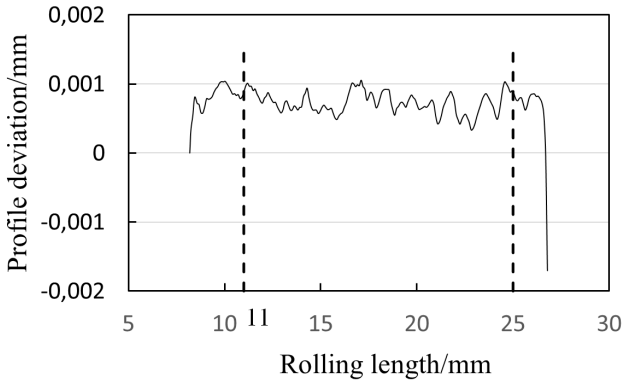

Fig.12. Tooth profile deviation curves obtained experimentally.

As shown in Table 5., the total profile deviation results of the 13 groups' tooth profile fluctuate between 0.54 um and 0.80 um; the form deviation results of the 13 groups' tooth profile fluctuate between 0.48 um and 0.68 um; the slope deviation results of the 13 groups' tooth profile range from -0.16 um to 0.18 um.

To observe the difference between the measured results and the calibration values, we calculated the mean values of the 13 groups of total profile deviation, profile form deviation and profile slope deviation, respectively, 0.66 um, 0.60 um and 0.03 um, as shown in Table 5. The calibration values of total profile deviation, profile form deviation and profile slope deviation are 0.5 um, 0.5 um and 0 um, respectively. The difference between their mean values and calibration values are 0.16 um, 0.10 um and 0.03 um. The total deviation of tooth profile is the synthesis of the profile form deviation and the profile slope deviation, so we have only drawn the profile form deviation and profile slope deviation of the measurement results. The difference between their mean and calibration value are shown in Fig.13 and Fig.14.

Table 5. Measurement results of involute tooth profile deviation.

	Total profile deviation /um	**Profile form deviation** /um	**Profile slope deviation** /um
1	0.66	0.58	0.04
2	0.60	0.52	-0.06
3	0.54	0.48	-0.16
4	0.66	0.66	0.02
5	0.66	0.58	-0.12
6	0.70	0.66	0.04
7	0.70	0.64	0.1
8	0.80	0.58	0.16
9	0.70	0.66	0.04
10	0.66	0.64	0.06
11	0.56	0.56	0.18
12	0.64	0.62	0.14
13	0.68	0.68	0
Mean value	0.66	0.60	0.03
Calibrated value	0.5	0.5	0

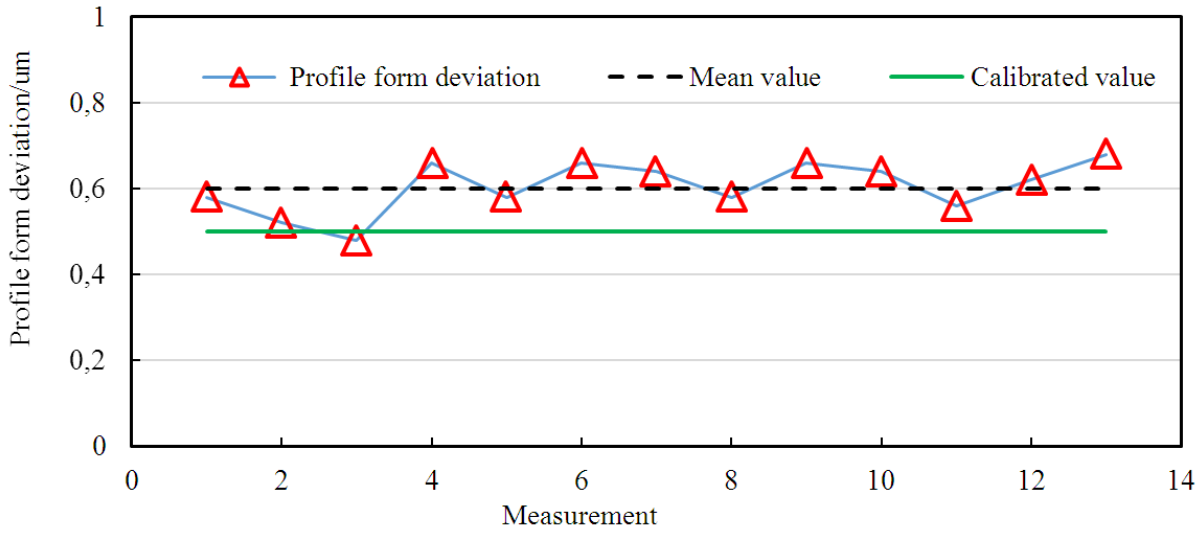

Fig.13. Measurement results of profile form deviation.

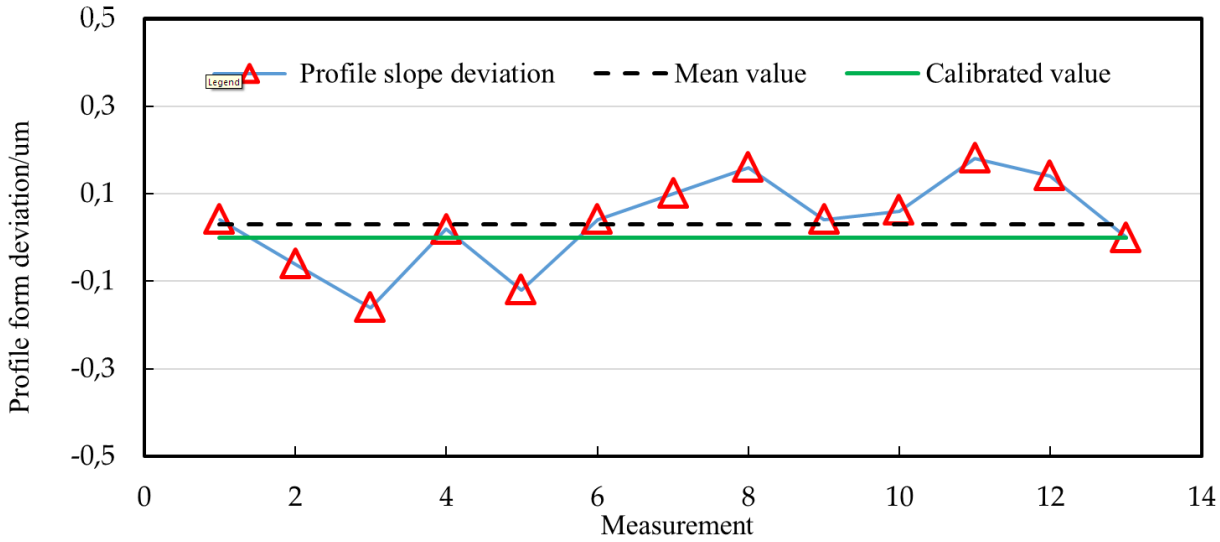

Fig.14. Measurement results of profile slope deviation

5. DISCUSSION

According to experimental measuring results, the mean value of the standard involute master tooth profile's total deviation measuring results show a difference of 0.16 um from the calibration value, shape deviation a difference of 0.1 um, slope deviation a difference of 0.03 um, all within a submicron difference. Those deviations are caused by the GMI itself. Therefore, the experiment verifies the accuracy of the GMI's measuring software, which includes the tooth profile measuring software. The experiment results were in good agreement with simulation results, which show that the proposed VGMI system can be used to test the accuracy and validity of the involute tooth profile measuring software.

The proposed VGMI system can analyze and evaluate the measuring software errors independently. The simulation results of tooth profile deviation can not only reflect the overall performance of the profile measurement results, but also reflect the details of the error curve. The error of the profile error curve is caused by the error of the model and the resolution of the sampling system. For example, the total deviation value of model 1 tooth profile is 14.90 um, and the error of the model error of 0.5 um is 0.48 um, which is within the range of the sampling error of 14.52 um. The value of each point on the error curve is the result of the combined effect of the model error and sampling error. However, the physical measurement can only prove the validity in terms of the whole measuring system and the analysis can only be done towards the overall index of the measuring results. The error curve from experiments shown in Fig.12. can hardly be analyzed in detail, and the error may be the result of the comprehensive effect of the mechanical system, the probe detection error, the workpiece error, the environmental error, the installation error and so on.

The VGMI system uses triangle model error controllable as digital master, which can be used to simulate any workpiece model, such as spiral bevel gear, hourglass worm and other complex workpieces which are difficult to manufacture as the standard workpiece. The measurement software of this kind of complex workpiece can still be tested, which can solve the problem that the measurement software is not solved in the case of no calibration workpiece in literature 12.

6. CONCLUSION

1. The proposed VGMI can test the correctness of the measuring software independently and the triangular patch model is quite suitable for software test. In this paper, the correctness of the tooth profile measurement software is verified by simulation and experiment.
2. VGMI can separate the error in the measurement result of the measurement software. Taking the tooth profile measurement as an example, VGMI can separate the workpiece model error and sampling system error in the profile error curve, and the actual measurement makes it difficult to quantitatively analyze the error source in the measurement results.
3. The VGMI provides a new theoretical platform for measuring software verification of spiral bevel gear, hourglass worm and other complex workpieces which are difficult to manufacture as standard artifacts.

ACKNOWLEDGMENT

This research was supported in part by the National Natural Science Foundation of China (Grant No.51475351), the Project Supported by Natural Science Basic Research Plan in Shaanxi Province of China (Program No. 2015JM5190) and the Key Laboratory Open Fund of Non-traditional Machining in Shaanxi Province of China (Grant No. ST-12013). The first author would like to thank Prof. YangQuan Chen for language editing.

REFERENCES

[1] Acko, B., Mccarthy, M., Haertig, F., Buchmeister, B. (2012). Standards for testing freeform measurement capability of optical and tactile coordinate measuring machines. *Measurement Science & Technology*, 23 (9), 94013-94025.

[2] Frazer, R.C. (2007). *Measurement uncertainty in gear metrology*. Doctoral dissertation, Newcastle University, UK.

[3] Greif, N. (2006). Software testing and preventive quality assurance for metrology. *Computer Standards & Interfaces*, 28 (3), 286-296.

[4] Nieciąg, H. (2012). The assessment of the criterion in tests of acceptance type of the metrological software in coordinate measuring systems. In *10th International Scientific Conference "Coordinate Measuring Technique"*, 23-25 April, 2012, Bielsko-Biała, Poland.

[5] Greif, N., Richter, D. (2009). Software validation and preventive software quality assurance for metrology. In *Data Modeling for Metrology and Testing in Measurement Science*. Birkhäuser Basel, 1-41.

[6] Härtig, F., Rost, K., Goch, G. (2010). Large gear material standard for the traceability of gears for transmission manufacturing. In *International Conference on Gears*, 4-6 October, 2010, Technical University of Munich, Germany, 991-1004.

[7] Komori, M., Takeoka, F., Kondo, K., Kondo, Y., Takatsuji, T., Osawa, S., Kubo, A. (2010). Design method of double ball artifact for use in evaluating the accuracy of a gear-measuring instrument. *Journal of Mechanical Design*, 132 (7), 071010.

[8] Levenson, M.S. (2000). Performance measures for geometric fitting in the NIST algorithm testing and evaluation program for coordinate measurement systems. *Journal of Research of NIST*, 100 (5), 563-574.

[9] Nieciąg, H. (2015). Improvement of simulation method in validation of software of the coordinate measuring systems. *Measurement Science Review,* 15 (5), 226-235.

[10] Zhang, R.J., Wang, G.J. (2008). The sharp upper bound on the distance between a parametric patch and its interpolated triangle. *Science in China, Series F: Information Sciences*, 51 (2), 113-119.

[11] Sladek, J.A. (2016). *Coordinate Metrology: Accuracy of Systems and Measurements*. Springer.

[12] Frank, H. (2007). Necessity and benefit of certified software--practical experience gained with commercial involute gear evaluation software. In *PTB-BIPM Workshop on the Impact of Information Technology in Metrology*, 5-7 June, 2007, Berlin, Germany.

[13] International Organization for Standardization. (2008). *Geometrical Product Specifications (GPS) - Acceptance and Reverification Tests for Coordinate Measuring Machines (CMM) - Part 6: Estimation of Errors in Computing Gaussian Associated Features*. ISO 10360-6.

[14] Taguchi, T., Kondo, Y. (2016). Evaluation of a high-precision gear measuring machine for helix measurement using helix and wedge artifacts. *Measurement Science & Technology*, 27 (8), 084008.

[15] Wäldele, F., Bittner, B., Busch, K., Drieschner, R., Elligsen, R. (1993). Testing of coordinate measuring machine software. *Precision Engineering*, 15 (2), 121-123.

[16] Takeoka, F., Komori, M., Takahashi, M., Kubo, A., Takatsuji, T., Osawa, S. (2009). Gear checker analysis and evaluation using a virtual gear checker. *Measurement Science & Technology*, 20 (4), 1-11.

[17] Wichmann, B.A., Cox, M.G. (1992). Problems and strategies for software component testing standards. *Software Testing Verification & Reliability*, 2 (4), 167-185.

Received May 02, 2017.
Accepted August 11, 2017.